Origin and Nature of Spontaneous Shape Fluctuations in “Small” Nanoparticles

Ying Yang and Hao Zhang*

Department of Chemical and Materials Engineering, University of Alberta, Edmonton, Alberta T6G 2V4, Canada

Jack F. Douglas*

Materials Science and Engineering Division, National Institute of Standards and Technology, Gaithersburg, Maryland 20899, United States

ABSTRACT

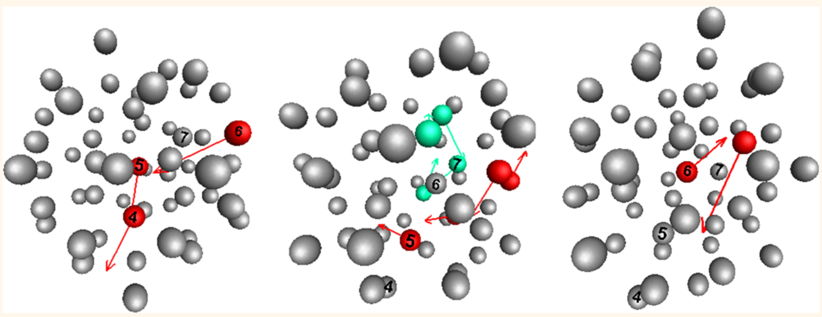

Normally chemically inert materials such as Au have been found to be catalytically active in the form of particles whose size is about 1 nm. Direct and indirect observations of various types of metal nanoparticles (NPs) in this size range, under catalytically relevant conditions for fuel-cell operation and catalysis, have indicated that such “small” particles can exhibit large *spontaneous shape fluctuations* and significant changes in shape and chemical activity in response to alterations in environmental conditions. NPs also normally exhibit facile coalescence when in proximity, impacting their stability and reactivity in applications. We perform molecular dynamics simulations on Ni nanoparticles, a commonly used NP in catalytic applications and carbon nanotube growth, in the $\approx$1 nm size regime where large-scale shape fluctuations have been observed experimentally. An analysis of the large-scale shape fluctuations observed in our simulations of these “small” NPs indicates that they are accompanied by collective motion of Ni atoms through the NP center, and we quantify these dynamic structures and their impact on NP shape. In contrast, stringlike collective atomic motion is confined to the NP interfacial region of NPs having a diameter greater than a few nanometers, and correspondingly, the overall NP shape remains roughly spherical, a case studied in our prior Ni NP simulations. Evidently, the large spontaneous NP shape fluctuations reflect a change in character of the collective atomic dynamics when the NPs become critically small in size.

KEYWORDS: nanoparticles · string collective atomic motion · molecular dynamics · nanoparticle shape fluctuations

Nanoparticles (NPs) undergoing spontaneous shape fluctuations have been the focus of numerous recent experimental studies. Most of these observations have been made for metallic NPs having relevance for catalysis applications such as Au,[1−4] Bi,[5,6] Pd,[7] Pt[8,9] Cu,[10] and Ni.[11] For example, Marchak *et al.*[5] observed spontaneous NP shape fluctuations in individual Bi NPs and associated NP property (band gap) fluctuations, and Helveg *et al.*[11] investigated the surface reorganization of Ni NPs in the course of their observations on carbon nanotube growth from the surface of these NPs. Continuous shape changes of Au NPs having a radius of about 1 nm have been observed by irradiation of these NPs with an electron beam,[7] and large shape changes have been found in Pd NPs during CO/NO cycling of the environment around these NPs.[10] The observed sensitivity of NPs to their environment (*e.g.*, hydrostatic pressure, dispersing NPs with other metals, the presence of solvents, or even illumination) is

* Address correspondence to hao.zhang@ualberta.ca, jack.douglas@nist.gov.

Received for review May 21, 2014 and accepted July 3, 2014.

Published online July 03, 2014
10.1021/nn502767t

consistent with a high interfacial atomic mobility in these NPs, and the intuitive concepts of "surface melting"[12] and "quasi-liquid layer"[13,14] have often been invoked to rationalize this phenomenon. Kang *et al*.[15] have alternatively described Al_{55} clusters as being "half-solid" because of the high mobility of the surface atoms in these small NPs. Zhang *et al*.[16] have noted the existence of an unexpected solid-to-solid structural transition below the melting temperature in Ni NPs having about 900 atoms, while the dynamics of NPs with more atoms could be characterized as "surface premelting" on a solid crystalline core. Uppenbrink and Wales[17] investigated the clusters of 13−150 Lennard-Jones atoms and found that different capping layers could greatly affect the stability of the particles. Wales and Munro[18] further studied the morphology change between icosahedra, cuboctahedra, and decahedra in metal clusters with 13, 55, and 147 atoms (magic number) and found that cooperative rearrangement of atoms was responsible the NP structural changes in these small NPs. Interestingly, the rearrangements found in these studies occur *via* a single transition state, while those in larger NPs[19] studied later occurred through a sequence of transition-state events. However, exact nature of atomic motions in this liquid-like layer of NPs and the fundamental causes of the shape fluctuations in small solid NPs have not been investigated before, either computationally or experimentally.

Observations of large shape changes in NPs genuinely nanoscopic in size suggest that there is more to the chemical activity of NPs than just high interfacial mobility and surface area. In many cases, shape fluctuations in small NPs are dynamically reversible, as well as facile, leading to fluctuating "on-and-off"[20] changes in catalytic activity and optical properties ("blinking'), pointing to the practical significance of this phenomenon for applications in materials science and biology.[21−23] What is the origin of these shape fluctuations and associated property fluctuations in small NPs?

One of the established characteristics of small NPs is their capacity to undergo dynamic transitions between rigid solid-like and liquid-like states. This dynamic coexistence phenomenon was first observed in simulations of noble gas clusters of Ar[24,25] and metallic atomic clusters of Al,[26] Au,[27] Ag,[28] and Ni.[29,30] Highly correlated motion of the atoms in the form of permutational atomic collective motion[25,31] was also observed accompanying the shape fluctuations, but this collective motion, and its significance in relation to particle shape fluctuations, was not quantified in these pioneering studies of atomic cluster dynamics. The primary purpose of the present paper is to investigate this phenomenon quantitatively, drawing on methodologies drawn from recent studies of glass-forming liquids to determine the nature of collective atomic motions responsible for the NP shape fluctuations.[32,33]

Previously,[34] we focused on relatively large Ni NPs having a diameter of about 4 nm (N = 2899 Ni atoms) where large-scale NP shape fluctuations were not conspicuous. For these larger NPs, we found that the interfacial dynamics (at elevated catalytically relevant temperatures) were characterized by the formation of a "premelted" NP interfacial layer having a relatively high atomic mobility, while the crystalline NP core retained the ordering of a crystal. Although the structure of the interfacial layer of these surface-melted NP can be characterized as "amorphous", the dynamics of this "liquid-like" layer were found to be highly heterogeneous, closely resembling the dynamics of glass-forming liquids[32,33] and the grain boundaries of crystalline materials.[35] In particular, the molecular dynamics of the interfacial layer of the NPs, and other "glassy" materials involving strongly interacting and disordered materials, are characterized by stringlike correlated particle movements, *i.e.*, "strings".[36,37] A recent study provided similar evidence for the collective atomic dynamics in raft-like lipid membrane,[38] with the thickness of 5 nm. In our previous work, we also found that the "fragility" of the amorphous interfacial layer dynamics, a measure of the relative strength of the temperature dependence of diffusion and relaxation processes,[37,39,40] could be tuned by altering NP size and by alloying the Ni NP with other metallic species such as Au, Ag, Pt, *etc*. The recognition of these excitation structures provides insight into how the interfacial dynamics of NPs can be modulated with additives and by varying the geometrical structure of the nanomaterial. We note that this type of collective particle motion has been directly observed experimentally, *e.g.*, in ultrahigh resolution images of amorphous metal films of Ge,[12] in particle tracking measurements on colloidal hard sphere suspensions,[41,42] and by imaging the grain boundaries of colloidal crystals.[43,44]

In the present work, we explore NP shape fluctuations in a single isolated Ni NP having a radius, $r \approx 1$ nm. In particular, we find that Ni NPs having r = 0.8 nm undergo considerable shape fluctuations over an appreciable temperature (T) range near the melting temperature (T_m), while larger NPs (r > 1 nm) fluctuations show little departure from an average spherical particle shape. We examine T_m and other basic properties of the NPs before investigating their surface, interfacial, and inner NP core dynamics in the vicinity of T_m. Specifically, we investigate fluctuations in the NP potential energy, Debye−Waller factor, and shape changes of the NP through determination of the radius of gyration tensor of the NP as a function of time. We find that shape fluctuations are accompanied by large displacements of the central atoms within the NP that trigger the large-scale particle shape fluctuations. These shape fluctuations are facilitated by stringlike collective motion taking a novel form, the migration of atoms through the *center* of the NP. In other words,

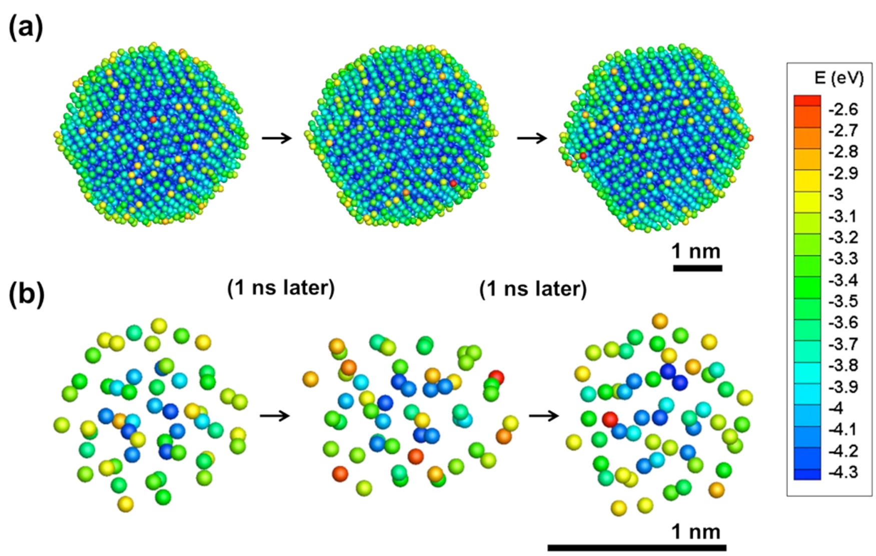

Figure 1. NP shape evolutions for (a) $N = 2899$ at 1200 K (0.8 T_m) and (b) $N = 55$ Ni NPs at 1200 K (0.98 T_m). The shape fluctuations and stringlike collective atomic motion are largely confined to the interfacial layer in the large NP. In contrast, large shape fluctuations arise at equilibrium in the smaller NP associated with coordinated displacements of the Ni atoms through the center of the NP. Atoms are colored by potential energy.

when the NPs become critically small in size the stringlike collective molecular motion observed in the interfacial region of larger NPs (see Figure 2 of Zhang *et al.*[34]) no longer remains localized to the NP interfacial region. Instead, the strings "short-circuit" by passing through the NP center, a phenomenon that is highly disruptive to NP shape.

RESULTS AND DISCUSSION

A. Initial Qualitative Look at "Small" Nanoparticle Shape Fluctuations. In previous work,[34] we studied Ni NPs having an average particle diameter >4 nm and found no large-scale NP shape fluctuations for such large particles at any T. Figure 1a illustrates this type of NP as a reference point in our discussion below. We see that while there are small-scale NP fluctuations in the interfacial layer thickness, the overall NP shape does not change appreciably from a roughly spherical shape. The melting temperature T_m for this reference "large" NP equals T_m = 1500 K, which can be compared with T_m = 1624 for a bulk Ni crystal[45] ($N \rightarrow \infty$), based on this potential.[34] The Voter–Chen potential is evidently not optimized to reproduce the bulk T_m since the observed T_m for Ni is almost 100 K higher than our simulation estimate, T_m(bulk) = 1728 K. We do not expect this discrepancy to affect our qualitative conclusions regarding the nature of shape fluctuations in small NPs, however.

We now contrast the shape fluctuations dynamics of these relatively large NPs to those of a "small" NP having a radius <1 nm (such NPs might be better termed "clusters" rather than NPs, but this is within size range found in catalytic applications of NPs). It is apparent from Figure 1b that our "small" Ni NPs indeed exhibit large-scale shape fluctuations reminiscent of those found previously for Ar atomic clusters by Berry and Wales, where the Ar interaction was described by a simple LJ potential.[46,47] Given the insensitivity of this fluctuation phenomenon to the type of intermolecular interaction, we expect these NP shape fluctuations to be a *generic* phenomenon, extending perhaps to organic nanoparticles, *i.e.*, proteins.

The shape fluctuations in these small NPs apparently involve significant collective atomic motion within the center of the NPs so their dynamics is *qualitatively different* from larger NPs (Figure 1a) where collective motion in the form of strings (the atoms move sequentially in this illustrative case, but stringlike motion does not generally have this character in glass-forming liquids, and we expect that the coherence of collective motion depends on temperature generally) was prevalent in the "premelted" NP interfacial layer; see Figure 2 of Zhang *et al.*[34] This singular form of collective motion was also noticed in previous simulations of the dynamics of small Ar clusters,[25] Au clusters,[18] and some other transition-metal clusters[19] (*i.e.*, Ag, Au, and Ni) where the cooperative motions were found to have a sequential nature. The principal focus of the present work is the quantification of the shape fluctuations and their relation to stringlike atomic cooperative motion within small NPs, where the detailed nature of the collective motion, sequential or otherwise, is not considered because this will require many further computations. First, we characterize the NP thermodynamic state so that comparisons of NPs having different size can be made at the same absolute temperature.

B. Nanoparticle Melting Temperature, T_m. All of our NPs are simulated starting from a particle having a bulk Ni fcc lattice structure, but with specific cutoff radius where the surrounding is a vacuum. The current study

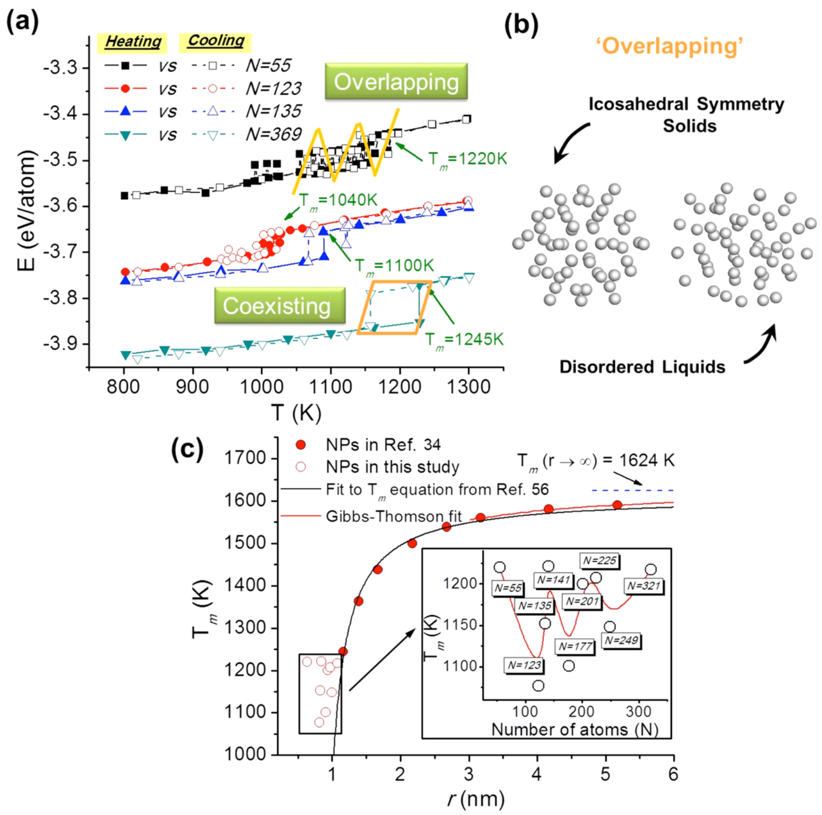

Figure 2. (a) Ni NP potential energy dependence on T for N = 55, 123, 135, and 369; (b) NP configurations corresponding to solid and liquid states; (c) melting point as a function of NP size.

considers NPs with 55 atoms (with diameter d = 1.07 nm), 123 atoms (d = 1.40 nm), 135 atoms (d = 1.45 nm), and 369 atoms (d = 2.03 nm), but we particularly focus on a small Ni NP having 55 atoms.

Although we started our simulations with particles having an fcc lattice structure, the small NPs quickly transformed into icosahedral solid structures when $N <$ 170 atoms. The observation that small metal NPs adopt low icosahedral or other noncrystallographic symmetries has been discussed in numerous experimental and computational studies. The reason is that the potential energy in this type of particle packing is lower than the fcc packing of the bulk crystal. Bulk crystals simply cannot exist in such dense packings and at some point ordered form must make a transition from icosahedral to thermodynamically "acceptable" crystal packing, which is fcc for Ni and many other metal atoms. For instance, Davis *et al.*[24] showed that 13-particle Ar clusters possess icosahedral symmetry below melting temperature. Sun and Gong[48] have demonstrated that small Al clusters exhibit magic number clusters, *i.e.*, Al13, Al55, and Al147, in which an icosahedral-like symmetry describes the lowest energy structure; however, an octahedral symmetry can be a stable structure for other nonmagic number metal atom clusters. In addition, we expect the starting fcc crystal structure has limited effect on our simulation results. Although in the "small" NP size regime (*e.g.*, $N <$ 200 atoms) a local fcc structure has a relatively high energy and is energetically unfavorable compared to the Mackay icosahedra,[17,18] the thermal energy is high enough in the regime (T in the range from $0.8T_m$ to T_m) we studied to quickly overcome the energy barrier between the fcc and icosahedra structures, which brings the system from the highly nonequilibrium fcc state to equilibrium or near-equilibrium state. However, the starting structure effect must certainly become relevant at lower T where the probability of getting trapped in a nonequilibrium state is much higher.

We next determined T_m to facilitate the comparison of the dynamics of NPs having different sizes. The NP potential energy changes upon heating, as illustrated in Figure 2a, and T_m is determined as the point where the NP becomes completely liquid, signaling a transformation from an ordered solid to a disordered liquid. The looplike potential energy curve obtained from a heating and cooling cycle provides evidence for "dynamic coexistence" in these small NPs, a phenomenon investigated previously.[49−53] While this coexistence phenomenon occurs for several cases considered (N = 135, 369), for N = 55 and 123, the heating and cooling curves continuously go up and down within the transitional T range. Under these conditions, the differentiation of the solid and liquid states becomes ambiguous, motivating the introduction of the term "overlapping" regime to describe this "twilight zone"

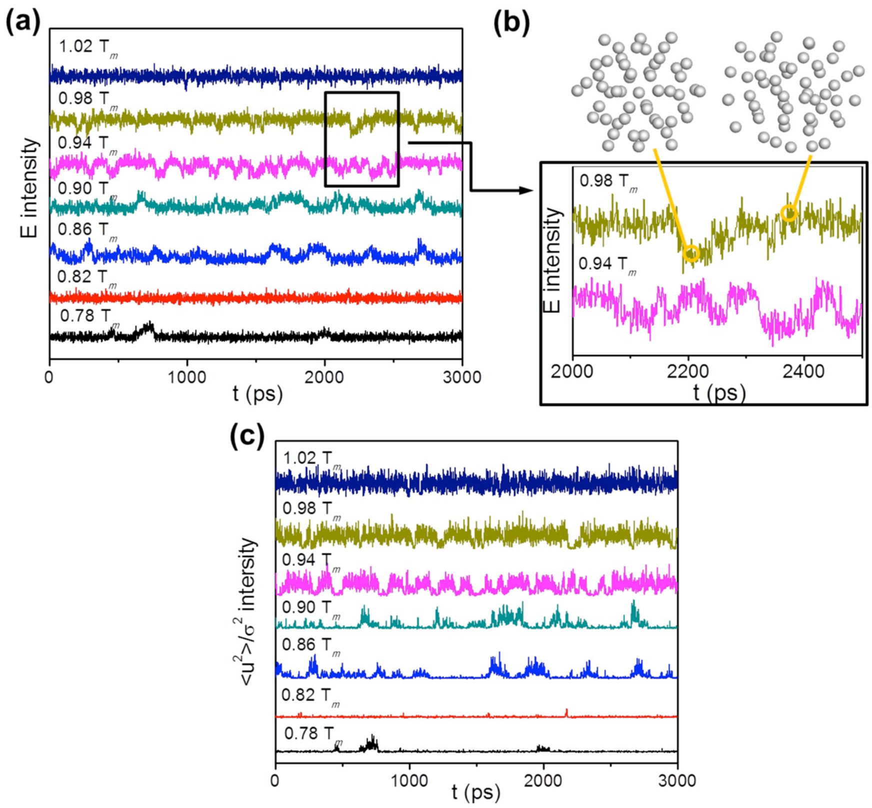

Figure 3. (a) Ni NP potential energy, (b) magnified region, and (c) reduced DWF $<u^2>/\sigma^2$ on dependence on T for N = 55.

NP state. With a decrease of NP size, the melting and cooling curves change from dynamic coexistence to the "overlapping" regime. NP configurations corresponding to N = 55 are shown in Figure 2b, where we see an odd form of melting in which the NP transforms from a crystal having icosahedral symmetry solid to a disordered liquid during heating and freezes into an icosahedral symmetry solid upon cooling. Meanwhile, the change from dynamic coexistence to phases in contact has been analyzed in detail in previous work and is well understood.[54] In small systems, the energetic cost of the interface is too large, and dynamic coexistence results, which is also characterized by an S-bend in the microcanonical caloric curve.[54]

Our previous studies of T_m as a function of NP size indicated that ΔT_m varies approximately inversely with the NP radius when the NPs are relative large (N > 10000 or 6 nm), conforming to the expectations of the Gibbs–Thomson relationship.[34,55] However, even this earlier work indicated deviations from continuum theory estimates of T_m when the NPs became relatively small (N < 700 or 2.5 nm), but these deviations were left unexplained at the time (see Figure 1 of Zhang *et al.*[34]). Here, these T_m plots are updated (Figure 2c) to include data for smaller NPs.

To gain an insight into the onset of this noncontinuum NP regime, we first plotted the previous Gibbs–Thomson curve in Figure 2c for reference. Then we attempted a fit of our extended T_m estimates to a melting model that addresses observed NP size-dependent changes in the amplitude of the Debye–Waller factor,[28] in conjunction with the Lindemann melting criterion,[56] to estimate T_m. This model indicated a modified scaling for the T_m shift with NP radius, *i.e.*, $(T/T_m) \approx \exp(A/(r-R_c))$, where A is a constant and R_c is a "critical NP radius" and recovers the continuum limit scaling of $T_m(r)$ when the NPs are larger than N = 141 or 1.5 nm. Although this modified model of T_m also breaks down when the NPs become very small, the critical radius R_c obtained from a numerical fit of our T_m data to this model corresponds closely to the scale at which large NP shape changes become prevalent in our simulations.

The inset of Figure 2c shows the more complicated changes in T_m with the number of Ni for NPs around R_c. In particular, T_m oscillates for "small" NPs (N < 369), revealing a "magic number" phenomenon associated with appreciable changes of the NP free energy with the addition of individual atoms.[57] This is a generic feature of small NPs[58] that is seen both in experiments and simulations;[57,59] the peaks in the T_m values normally occur close to the atomic number N values (13, 55, 147, 309, ...) at which point the NP form highly stable Mackay icosahedron structures at low T.[60,61] These magic number T_m values are thus the consequence of the formation of well-packed small clusters at low temperatures for particular numbers of atoms.[58]

C. Potential Energy and Debye–Waller Factor. Figure 3 shows fluctuations in E_{tot} (Figure 3a) and $<u^2>$

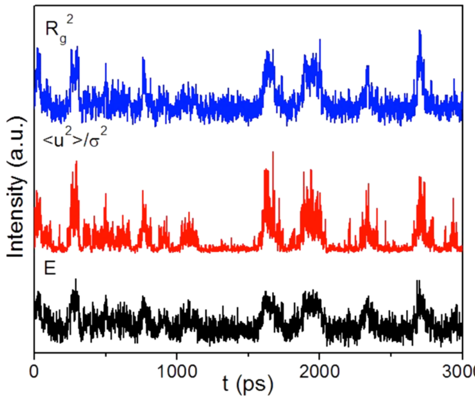

Figure 4. Potential energy, relative $<u^2>$, and R_g as a function of t for $T = 0.86T_m$ and $N = 55$.

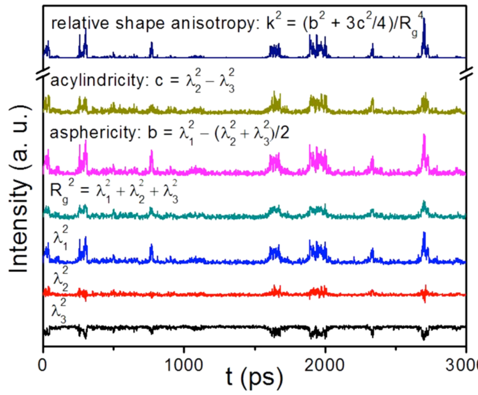

Figure 5. Dependence of R_g and shape factors of a Ni NP on t for $T = 0.86T_m$ and $N = 55$.

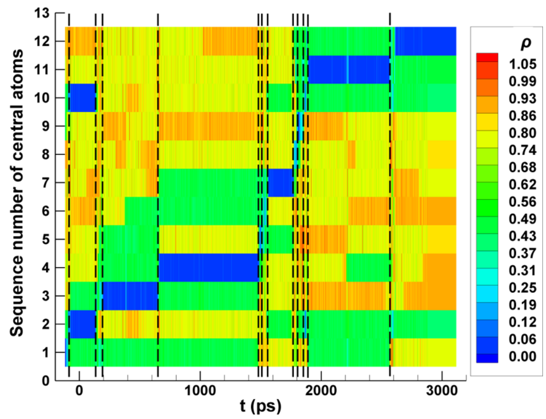

Figure 6. Dynamic atomic positions of sequential central atom positions as a function of t for $0.86T_m$ and $N = 55$.

(Figure 3c) as a function of t and for a range of T. At relatively low T, *e.g.*, 950 K (0.78 T_m) and 1000 K (0.82 T_m), the fluctuations in E_{tot} and $<u^2>$ are small, reflecting the stability of the NP. At relatively high T, *e.g.*, T = 1250 K and T/T_m = 1.02, E_{tot} and $<u^2>$ both exhibit large fluctuations. These fluctuations can be seen more clearly in Figure 3b, with the representative configurations illustrated for solid and liquid states. In the coexistence range, which is between 1050 K ($0.86T_m$) and 1100 K ($0.90T_m$), E_{tot} and $<u^2>$ fluctuate between two distinct energy states in the T regime as the NP undergoes significant shape changes. Some intermittent transformations between these solid- and liquid-like dynamic states occurs at almost all T simulated. We next consider how these shape fluctuations are related to fluctuations in E_{tot} and $<u^2>$.

D. Correlation of Nanoparticle Shape and Energy Fluctuations. We focus on the representative temperature 0.86 T_m for the N=55 Ni NP in the overlapping regime. In Figure 4, we observe two-level $E_{tot}(t)$ fluctuations that are directly correlated with the particle displacement fluctuations and with fluctuations in the NP radius of gyration, R_g^2. The baseline values of these properties are symptomatic of the solid state while the peak values of these properties are characteristic of the NP "liquid state". We quantify the NP shape fluctuations accompanying NP state changes through consideration of the NP shape parameters b, c, and k^2 defined above, and these properties are shown in Figure 5. At particular time events at which the particle starts changing its shape, the λ_i along each direction (i = 1, 2, 3) suddenly become unequal. Baselines in b and c then occur when the NP returns to its original near-spherical shape. The shape factor k^2 quantifies the NP shape anisotropy that accompanies these "quake" events. Evidently, the shape fluctuations are directly correlated with the NP energy and DWF fluctuations.

E. Molecular Dynamic Origin of Nanoparticle Shape Fluctuations. Now that we have established that small NPs undergo striking shape changes below their melting temperature, it is natural to consider what role collective atomic motion might play in this process. This leads us to focus on the central position of the NP for N = 55 where the scale of atomic motion can be peculiarly large for small NPs[62] (Jellinek observed that $<u^2>$ in the center of the particle can actually be *maximal* in the dynamic coexistence regime, reflecting the fact the central particle is constantly being kicked out of the cluster center[63]). As explained in the Simulation Methodology section, we calculate the mean first-passage time for atoms to reach the surface of the NP. The value of ρ for any given atom provides information on the relative rate at which particles within the NP emerge on the NP surface as a function of various starting points within the NP.

Within the time period of 3000 ps, we show in Figure 6 the evolution of the atomic position of the central particle as it makes its way to the NP surface. The central atomic position changes 12 times in this time period, and these events are labeled 1−12 in Figure 6. Note that "2" and "10" are the actually the same atom, meaning this atom moves in this way twice so there is some back and forth motion of the atoms. The displacement instants are marked by a dashed line.

To clarify how the NP shape change are synchronized with the displacement of the central NP atoms,

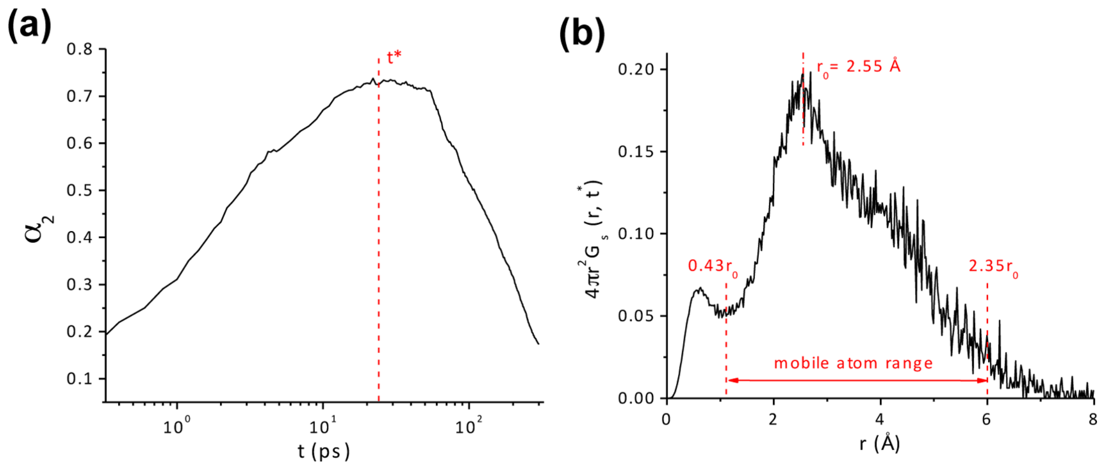

Figure 7. (a) Non-Gaussian parameter NGP (α_2) and (b) van Hove function G_s (r, t*) for N = 55 at T = 0.86T_m.

we created an animation of the NP evolution for the time period between 1800 to 1900 ps; see the video in the Supporting Information. In the movie, the central atoms labeled as "7″, "8" ,and "9" are based on the corresponding numbers in Figure 6. This visualization shows the colored atom "7" initially at the NP center and then "8" and "9" follow its movement to the NP surface, followed by a large NP shape change.

F. Stringlike Collective Motion. What kind of atomic motion underlies the NP shape fluctuations? Are they moving incoherently or coherently like a crystal or does the motion have some "in-between" or "mixed" character as in former simulations of the interfacial dynamics of larger NPs where the motions had a stringlike form? To answer these questions and to quantify the collective nature of the motion in these NPs we look for stringlike collective motion, a characteristic mode of molecular displacement in strongly interacting disordered materials. Previous studies also considered the precise nature of the stringlike "correlated" motion, where two extremes seem to exist, sequential or concerted movement, and these can be distinguished by suitable analysis of the pathways.[64] This later work indicated that highly cooperative large-scale NP shape changes in larger particles correspond to single transition states that can be broken down into a series of transition states with intervening local minima.

As in our former studies, our analysis of correlated atomic motion requires the determination of the non-Gaussian parameter α_2 and van Hove correlation function G_s (r, t) before the extent of collective motion can be inferred, and these details for the present system are described in the Supporting Information since this analysis has been described repeatedly in previous publications.[34,37,65]

The non-Gaussian parameter α_2 and G_s (r, t) for the N = 55 NP at 0.86T_m are shown in Figure 7. The peak position of α_2 occurs at 24 ps, and substituting t* into G_s (r, t) reveals a classic hopping peak at 2.55 Å. There is then clear evidence of dynamic heterogeneity in

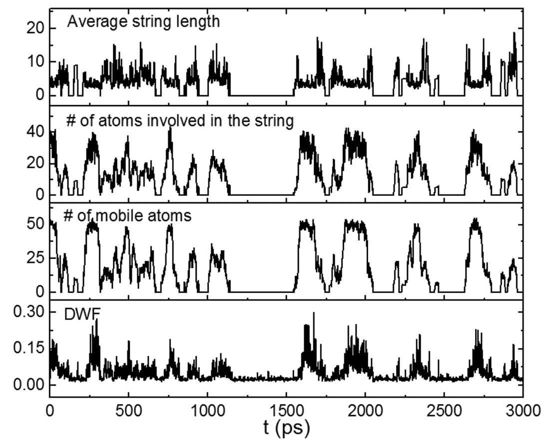

Figure 8. Numbers of mobile atoms, string atoms, and string length compared with <u^2> as a function of t for N = 55 and T = 0.86T_m.

the dynamics of the Ni atoms in these small clusters. The "mobile" atom cut-off range is fixed by the dashed line and ranges from 0.43r_0 to 2.35r_0.

If mobile atoms in the form of stringlike cooperative atomic rearrangements are responsible for the peak in α_2 and the hopping peak in G_s (r, t), as in previous studies of larger Ni NPs, then we should see particles moving, but staying within proximity of each other rather than wandering off on their own. Using criteria explained in Supporting Information and our previous papers,[34,37,65] the extent of stringlike collective motion is then determined and the results of this analysis are shown in Figure 8. The majority of collective motion events observed in the current study is sequential, but we need to be careful in drawing general conclusions about the nature of the collective motion from these limited observations. As can be seen, the relative shape anisotropy, the number of mobile atoms, the number of atoms involved in the string, and the string length peak positions all match each other rather well. Stringlike collective motion clearly accompanies the NP shape changes.

Further comparison for the string length with fluctuations in the shape anisotropy (shown by dashed line

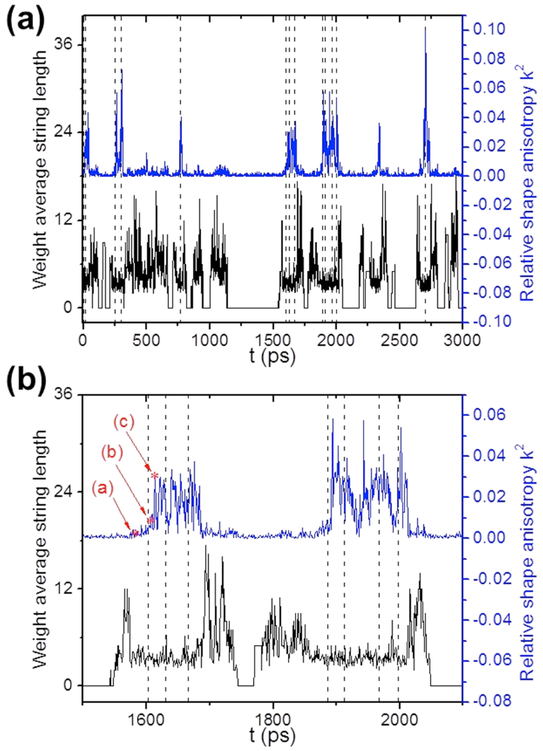

Figure 9. (a) Comparison of string length L, central atom displacement, and shape anisotropy k^2, and (b) details of those from 1500 to 2100 ps.

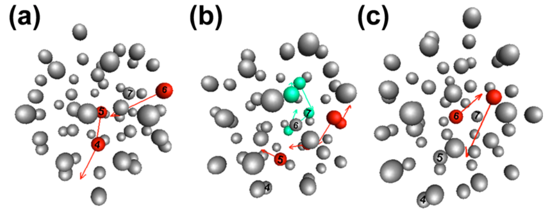

Figure 10. Configurations of N = 55 Ni NP at $T = 0.86T_m$ for (a) 1583 ps, (b) 1607 ps, and (c) 1614 ps.

in Figure 6) is presented in Figure 9(a). Apparently, these events of coordinated atomic movement do not quite happen at exactly the same time as the shape fluctuation events. Instead, we see that the longest strings appear just before and after the peaks in the NP. Short strings occur without large-scale particle shape fluctuations. Further, there is little string activity when the particles are in their solid state, as found in our previous paper on larger NPs.[55] The longer strings have an erratic fluctuating length and these collective atomic movements are strongly correlated with the NP shape fluctuations. These longer strings are highly reminiscent of fluctuating strings found in the interfacial region between ordered and ordered particle regions of a larger Ni NPs (∼2 nm radius; N = 2899) under *nonequilibrium* melting or freezing conditions.[65] The stringlike collective motion apparently facilitates the local state transformation from the "liquid" or dynamically "mobile" and the "solid" to "dynamically immobile" particle states.

A more detailed examination of this interconversion process in the time regime between 1500 and 2100 ps is shown in Figure 9(b). Meanwhile, in order to make a clearer demonstration for this process, a comparable video is available in the Supporting Information. We see that after long strings form in an initially solid-like NP configuration no shape change occurs, while the number of atoms involved in the string can have a value as large as 40. The central atom displacement occurs only when the number of atoms involved in the string is large, but the string length is relatively small, pointing to a particular significance for intermediate size strings in the shape transformation process. The shape anisotropy parameter k^2, step by step, reaches a maximum in three stages corresponding to 1583, 1607, and 1614 ps. These events are labeled as (a), (b), and (c) in Figure 9(b).

We can now effectively describe how the string motion actuates the cluster shape changes. Figure 10 shows those three configurations at the three stages of time development mentioned above. This perspective view helps us distinguish atoms at the front and at the back of the NP. Different colors represent different string clusters involved in the collective motion where only the strings include central atoms are highlighted. The three central atoms are labeled "5", "6", and "7" subsequently, with another string atom labeled "4", according to the number depicted in Figure 7. In the first window, "6" is on the outer surface, preparing to replace atom "5", and this exchange is orchestrated by a string collective displacement, the positions and configuration of which are shown in the second time window at 24 ps (the time t^* at which the non-Gaussian parameter peaks). In this snapshot, atom "5" initiates another string movement and atom "7" starts then participates in a string event. In the third time window, where we observe the largest shape change, the central atom "6" moves through the initiation of a new string and similar string motions and shape changes occur during other time periods. The string motion is apparently "initiated" by activating particles in regions of high mobility and presumably high local instability; in practice, this can mean regions of *high density* and *low free volume* rather than regions of low density and high free volume. Free volume is not a general correlate with mobility on a local scale, a point made before in glass-forming liquids.[32,33,64,66]

Finally, to confirm that the shape changes are directly related to the large displacement of the central atom of the NP, we carried out another simulation where the 5 atoms in the center of the NP are fixed in position by setting their temperature to 0 K, and representative simulations of this experiment are shown Figure 11. Almost no shape anisotropy arises in the NPs when the core is fixed in this way. The shape changes reflect the disruptive effect of the central atom migration to the surface in our small NPs.

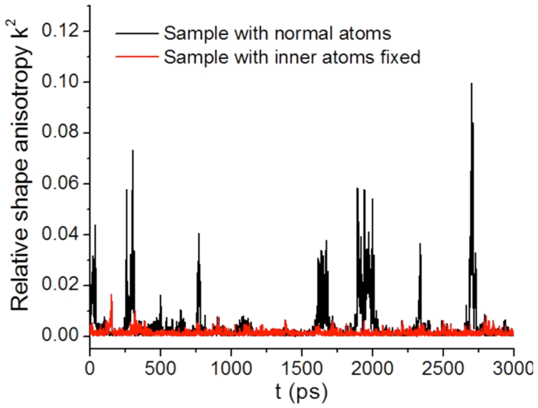

Figure 11. Comparison of relative shape anisotropy for unconstrained Ni NP having $N = 55$ and $T = 0.86T_m$ and a core-constrained NP.

CONCLUSIONS

We investigate NP shape fluctuations in a single Ni NP having a radius smaller than 1 nm using molecular dynamics simulation. Our representative small (0.8 nm) Ni NP undergoes considerable shape fluctuations in a wide temperature range near the melting temperature T_m. An examination of fluctuations in the NP potential energy, Debye–Waller factor, and measures of NP shape suggest that the shape fluctuations are accompanied by large displacements of the central atom within the NP that trigger the large-scale particle shape fluctuations. Once triggered, the coordinated atomic motion driving atoms from the NP core to the surface drives the large-scale shape fluctuations of the NPs.

These NP shape fluctuations are evidently reminiscent of the shape fluctuations of proteins and organic nanoparticles, and these fluctuations could have important implications in relation to NP transport and the unique catalytic properties of nanoparticles. There is evidence that the interfacial mobility and large shape fluctuations of small NPs probably play a significant role in the formation of crystal nuclei through the fusion and structural rearrangement of the relatively disordered "amorphous" prenucleation clusters,[67,68] and we expect an understanding of this type of fluctuating cluster to be essential for understanding the early stages of crystal growth that are not captured by classical nucleation theory. Such prenucleation "amorphous" clusters have been shown to play an essential role in biomineralization processes in bones and teeth[69−73] where collagen and self-assembling proteins form scaffolds on which NPs are organized. It also seems likely to us that the large shape fluctuations might aid in the intrusion of these NPs into the small scaffold pore spaces of collagen and other organic self-assembled template materials.[74,75] Large fluctuations in NP shape have also been suggested to contribute to the diffusion of small NPs.[76,77] Clearly, small inorganic nanoparticles can exhibit large configuration fluctuations, and fluctuations associated with chemical activity and properties, making these particles similar to proteins in many ways. This is natural given that proteins are just small *organic* nanoparticles. We plan to investigate the collective dynamics of folded globular proteins to see if they indeed exhibit a similar collective dynamics to that observed in our small Ni NPs.

Previous work and the current study mainly focus on atomic species with simple London dispersion interactions and simple many body potentials for metallic atoms system such as Ni. These atomic potentials are isotropic in nature, raising interesting questions about how particles with strong cohesive and anisotropic interactions, such as charged and dipolar particle systems, might influence this NP shape fluctuation phenomenon. In order to address these questions, we must qualify our results as applying to interaction potentials of the type we study. However, since the size and shape fluctuation are exhibited in variety of organic systems, we believe that materials exhibiting directional bonding should also exhibit such fluctuations. It is certainly true that simulations of atomics in charged glass-forming liquids exhibit stringlike collective motion as we have found in the present work. On the other hand, we may generally expect that the critical particle NP size at which the NP size fluctuations arise should depend on the cohesive interaction strength and on the presence of directional interactions, a point relevant to NPs involved in biomineralization. Further study is needed to confirm these expectations for NPs with such interactions. Finally, we point out that molecular dynamics simulations of water NPs having a size on the order of 1 nm[78] have indicated a large melting point suppression and dynamic coexistence between liquid and solid NP states, and we may naturally expect dynamic shape fluctuations in these NPs, a phenomenon of large potential relevance to the impact of these NPs on atmospheric chemistry.[78]

SIMULATION METHODOLOGY

Our simulations of Ni NPs are based on a potential derived by the embedded atom method (EAM),[79] a many-body potential that normally allows for more accurate crystalline metal material property, but at the expense of a greater cost in terms of required computer resources and time than two-body interaction potentials such as the Lennard-Jones (LJ) interaction potential and its variants. In the EAM method, the energy of the metal is estimated by embedding an atom into the local electron density field created by the atoms surrounding it and leads to the formal expression

$$E_{tot} = \sum_i F_i(\rho_{h,i}) + \frac{1}{2}\sum_i \sum_{j \neq i} \varphi_{ij}(R_{ij}),$$
$$\rho_{h,i} = \sum_{i \neq j} \rho_j^{\alpha}(R_{ij}) \qquad (1)$$

where $F_i(\rho_{h,i})$ is the embedded energy of atom i, $\varphi_{ij}(R_{ij})$ describes the pairwise interaction between atom i and j with the distance of R_{ij}, and $\rho_{h,i}$ is the electron density at atom i, contributed by other atoms j. As in the case of the simple pair LJ potential, the EAM potential involves a combination of short-range attraction and still shorter range repulsion.

We utilize the Voter–Chen EAM potential for Ni NP simulations since it yields the correct elastic constants, vacancy formation energy, cohesive energy, lattice parameter, interatomic spacing (properties to which it was fitted), and reasonable interface properties for Ni,[80] for example, the calculated surface energy for (100), (110), and (111) are 1760, 2002, and 1632 mJ/m^2, respectively, compared to experimental value for average face is 2280 ± 300 mJ/m^2. More importantly, the tendency of surface energy variation based on the specific surfaces, *i.e.*, γ (110) > γ (100) > γ (111), is in good agreement with results of other EAM potentials.[81] In addition, the surface relaxation simulation using this potential also shows that the percentage changes in interlayer spacing are in reasonable agreement with both LEED data and theoretical data.[82] Therefore, it is expected the Voter–Chen EAM potential for Ni is able to yield reasonable results on NPs with large surface-to-volume ratio.

The Ni NPs were initiated from an approximately spherical shape and a perfect local fcc structure. The NPs were first relaxed at room temperature for 1.5 ns with zero angular and linear momentum values. Note that while we start the NP with the fcc crystal structure of the bulk crystal, the NP for $N = 55$ quickly transforms to an icosahedral solid, which is the equilibrium structure of these smaller NPs.[29,60,83–85] In contrast, the crystal structure is maintained in the NP core for relatively large NPs.

The NPs were heated at a rate of 100 K/ns from room temperature (T = 300 K) until the NPs melted. Correspondingly, the melted NPs, obtained from the above heating history, were cooled at a rate of 100 K/ns from their melting conditions to room temperature. Although this rate of heating/cooling is relatively slow from the standpoint of molecular dynamics simulation, it is orders magnitude higher than the rates normally encountered in experimental studies. In order to probe kinetic processes that cannot be observed while heating at a continuous and high rate, we also performed "isothermal" heating studies. Isothermal simulations were performed where T was changed from 950 to 1250 K in discrete jumps of 50 K where T was held constant for 3 ns after each T jump.

We monitor the total potential energy E_{tot} for two purposes: (1) it provides a criterion for determining the transition between solid and liquid states and (2) it is an important property for characterizing the dynamics of the NPs because T_m, estimated from the T dependence of E_{tot}, allows us to define a reduced temperature T/T_m for comparison of NPs having different sizes.

Since it is anticipated that dynamics of nanometric NPs should share features with the interfacial dynamics of larger NPs[34] and glass-forming liquids,[32,33,39] we consider standard measures of dynamic heterogeneity in glassy materials such as non-Gaussian parameter α_2. This is a frequently considered measure of "dynamic heterogeneity" (DH) in glass-forming liquids.[31–36,43,86,87] In three dimensions, α_2 is defined in terms of even powers of displacement $r(t)$ of a atoms from their initial position at t = 0:

$$\alpha_2(\Delta t) = \frac{3\langle r^4(\Delta t)\rangle}{5\langle r^2(\Delta t)\rangle^2} - 1 \tag{2}$$

The non-Gaussian parameter α_2 is defined as equaling zero if the atomic motion is Brownian, and this measure of DH has often been considered in previous MD simulation studies of glass-forming liquids,[32,33] grain boundaries,[35] and the interfacial dynamics of NPs.[34] As in previous studies of larger NPs,[34] we observe collective motion taking the form of strings, and we describe our method for determining these dynamic structures in the Supporting Information since the same type of analysis has been described in several recent publications.[34–37] The ratio of the mean square atomic displacement $<r(t)^2>$ at a characteristic caging time on the order of 1 ps, or the "Debye–Waller factor" $<u^2>$, to the average distance between the atoms is another basic property utilized for characterizing the dynamics of glass-forming liquids,[32,33] and this quantity is often applied to roughly estimate the melting point of crystals[34] and to characterize the dynamics of NPs.[34] Its determination is also discussed in the Supporting Information.

Since fluctuations of NP shape are the primary concern here; we require a general measure of NP shape. The radius of gyration tensor provides an attractive choice for NP shape characterization and this quantity is often employed in the shape characterization of synthetic and biological macromolecules such as DNA and proteins.[88–90] The radius of gyration R_g is defined by[86,91]

$$R_g{}^2 = \frac{1}{N}\sum_i (r_i - r_{mass})^2 \tag{3}$$

where r_{mass} is the center of mass, and this quantity can be generalized by defining moments about different coordinate directions to define the R_g tensor.[87] The R_g tensor is symmetric in its components and can be diagonalized by rotating the particle to its principal axis orientation and the eigenvalues (λ_1, λ_2, λ_3) in the diagonal form of the R_g tensor and then provide a basis for NP shape characterization. Following common practice in polymer physics,[86,91] we define the NP asphericity b, acylindricity c, and relative shape anisotropy k^2 as

$$R_g{}^2 = \lambda_1^2 + \lambda_2^2 + \lambda_3^2 \tag{4}$$

$$b = \lambda_1{}^2 - \frac{1}{2}(\lambda_2{}^2 + \lambda_3{}^2) \tag{5}$$

$$c = \lambda_2{}^2 - \lambda_3{}^2 \tag{6}$$

$$k^2 = \frac{b^2 + (3/4)c^2}{R_g{}^4} \tag{7}$$

The simulations of the NP dynamics below reveal a basic event in the NP dynamics of significance in understanding the dynamics of these particles. At intermittent times, particles at various initial positions within the NP first emerge at the NP boundary, and we define a dimensionless variable ρ allowing for the identification of these events

$$\rho = \frac{1}{r_0}|r_i - r_{\text{mass}}| \tag{8}$$

where r_{i} is the position of specified atom i, r_0 is the initial radius, and r_{mass} is the center of mass of the NP. If $\rho \to 0$, the ith atom occupies the central position within the NP, while $\rho = 1$ indicates that this particle has emerged at the NP surface.

Conflict of Interest: The authors declare no competing financial interest.

Supporting Information Available: Methods for determining NP dynamic structures. Movie of NP shape fluctuation simulation. This material is available free of charge *via* the Internet at http://pubs.acs.org.

Acknowledgment. Y.Y. and H.Z. gratefully acknowledge the support of the Natural Sciences and Engineering Research Council of Canada under a Discovery Grant. J.F.D. acknowledges support of this work under an NIH grant (1 R01 EB006398-01A1).

REFERENCES AND NOTES

1. Li, Z. Y.; Young, N. P.; Di Vece, M.; Palomba, S.; Palmer, R. E.; Bleloch, a. L.; Curley, B. C.; Johnston, R. L.; Jiang, J.; Yuan, J. Three-Dimensional Atomic-Scale Structure of Size-Selected Gold Nanoclusters. *Nature* **2008**, *451*, 46–48.
2. Xu, W.; Kong, J. S.; Chen, P. Probing the Catalytic Activity and Heterogeneity of Au-Nanoparticles at the Single-Molecule Level. *Phys. Chem. Chem. Phys.* **2009**, *11*, 2767–2778.
3. Hughes, M. D.; Xu, Y.-J.; Jenkins, P.; McMorn, P.; Landon, P.; Enache, D. I.; Carley, A. F.; Attard, G. A.; Hutchings, G. J.; King, F.; et al. Tunable Gold Catalysts for Selective Hydrocarbon Oxidation under Mild Conditions. *Nature* **2005**, *437*, 1132–1135.
4. Bovin, J.; Wallenberg, R.; Smith, D. J. Imaging of Atomic Clouds Outside the Surfaces of Gold Crystals by Electron Microscopy. *Nature* **1985**, *317*, 47–49.
5. Marchak, D.; Glozman, D.; Vinshtein, Y.; Jarby, S.; Lereah, Y.; Cheshnovsky, O.; Selzer, Y. Large Anisotropic Conductance and Band Gap Fluctuations in Nearly Round-Shape Bismuth Nanoparticles. *Nano Lett.* **2012**, *12*, 1087–1091.
6. Marchak, D.; Glozman, D.; Vinshtein, Y.; Jarby, S.; Lereah, Y.; Cheshnovsky, O.; Selzer, Y. Molecular Control of Structural Dynamics and Conductance Switching in Bismuth Nanoparticles. *J. Phys. Chem. C* **2013**, *117*, 22218–22223.
7. Newton, M. A.; Belver-Coldeira, C.; Martínez-Arias, A.; Fernández-García, M. Dynamic *in Situ* Observation of Rapid Size and Shape Change of Supported Pd Nanoparticles During Co/No Cycling. *Nat. Mater.* **2007**, *6*, 528–532.
8. Narayanan, R.; El-Sayed, M. A. Shape-Dependent Catalytic Activity of Platinum Nanoparticles in Colloidal Solution. *Nano Lett.* **2004**, *4*, 1343–1348.
9. Yang, J.; Lee, J. Y.; Too, H.-P. Size Effect in Thiol and Amine Binding to Small Pt Nanoparticles. *Anal. Chim. Acta* **2006**, *571*, 206–210.
10. Hansen, P. L.; Wagner, J. B.; Helveg, S.; Rostrup-Nielsen, J. R.; Clausen, B. S.; Topsøe, H. Atom-Resolved Imaging of Dynamic Shape Changes in Supported Copper Nanocrystals. *Science* **2002**, *295*, 2053–2055.
11. Helveg, S.; López-Cartes, C.; Sehested, J.; Hansen, P. L.; Clausen, B. S.; Rostrup-nielsen, J. R.; Abild-pedersen, F.; Nørskov, J. K. Atomic-Scale Imaging of Carbon Nanofibre Growth. *Nature* **2004**, *427*, 426–429.
12. Feenstra, R. M.; Slavin, A. J.; Held, G. A.; Lutz, M. A. Edge Melting of the Ge(111) Surface Studied by Scanning Tunneling Microscopy. *Ultramicroscopy* **1992**, *42*, 33–40.
13. Krakow, W.; Jóse-Yacamán, M.; Aragón, J. Observation of Quasimelting at the Atomic Level in Au Nanoclusters. *Phys. Rev. B* **1994**, *49*, 10591–10596.
14. Ajayan, P.; Marks, L. Experimental Evidence for Quasimelting in Small Particles. *Phys. Rev. Lett.* **1989**, *63*, 279–282.
15. Kang, J.; Kim, Y. H. Half-Solidity of Tetrahedral-Like Al-55 Clusters. *ACS Nano* **2010**, *4*, 1092–1098.
16. Zhang, Z.; Hu, W.; Xiao, S. Melting, Melting Competition, and Structural Transitions between Shell-Closed Icosahedral and Octahedral Nickel Nanoclusters. *Phys. Rev. B* **2006**, *73*, 125443.
17. Uppenbrink, J.; Wales, D. J. Packing Schemes for Lennard-Jones Clusters of 13 to 150 Atoms: Minima, Transition-States and Rearrangement Mechanisms. *J. Chem. Soc., Faraday Trans.* **1991**, *87*, 215–222.
18. Wales, D. J.; Munro, L. J. Changes of Morphology and Capping of Model Transition Metal Clusters. *J. Phys. Chem.* **1996**, *100*, 2053–2061.
19. Wales, D. J.; Munro, L. J.; Doye, J. P. K. What Can Calculations Employing Empirical Potentials Teach Us About Bare Transition-Metal Clusters? *J. Chem. Soc., Dalton Trans.* **1996**, 611–623.
20. Zhou, X.; Xu, W.; Liu, G.; Panda, D.; Chen, P. Size-Dependent Catalytic Activity and Dynamics of Gold Nanoparticles at the Single-Molecule Level. *J. Am. Chem. Soc.* **2010**, *132*, 138–146.
21. Tao, A. R.; Habas, S.; Yang, P. D. Shape Control of Colloidal Metal Nanocrystals. *Small* **2008**, *4*, 310–325.
22. Savage, N. Trick of the Light. *Nature* **2013**, *495*, S8–S9.
23. Boyer, D.; Tamarat, P.; Maali, A.; Lounis, B.; Orrit, M. Photothermal Imaging of Nanometer-Sized Metal Particles among Scatterers. *Science* **2002**, *297*, 1160–1163.
24. Davis, H. L.; Jellinek, J.; Berry, R. S. Melting and Freezing in Isothermal Ar13 Clusters. *J. Chem. Phys.* **1987**, *86*, 6456–6464.
25. Wales, D. J. Transition States for Ar55. *Chem. Phys. Lett.* **1990**, *166*, 419–424.
26. Ojwang', J. G. O.; van Santen, R.; Kramer, G. J.; van Duin, A. C. T.; Goddard, W. A. Predictions of Melting, Crystallization, and Local Atomic Arrangements of Aluminum Clusters Using a Reactive Force Field. *J. Chem. Phys.* **2008**, *129*, 244506.
27. Baletto, F.; Mottet, C.; Ferrando, R. Molecular Dynamics Simulations of Surface Diffusion and Growth on Silver and Gold Clusters. *Surf. Sci.* **2000**, *446*, 31–45.
28. Baletto, F.; Ferrando, R. Island Adsorption and Adatom Diffusion on 3d Non-Crystalline Silver Nanoclusters. *Surf. Sci.* **2001**, *490*, 361–375.
29. Qi, Y.; Cagin, T.; Johnson, W. L.; Goddard, W. A. Melting and Crystallization in Ni Nanoclusters: The Mesoscale Regime. *J. Chem. Phys.* **2001**, *115*, 385–394.
30. Neyts, E. C.; Bogaerts, A. Numerical Study of the Size-Dependent Melting Mechanisms of Nickel Nanoclusters. *J. Phys. Chem. C* **2009**, *113*, 2771–2776.

31. Doye, J.; Wales, D. Structural Transitions and Global Minima of Sodium Chloride Clusters. *Phys. Rev. B* **1999**, *59*, 2292–2300.
32. Donati, C.; Glotzer, S. C.; Poole, P. H.; Kob, W.; Plimpton, S. J. Spatial Correlations of Mobility and Immobility in a Glass-Forming Lennard-Jones Liquid. *Phys. Rev. E* **1999**, *60*, 3107–3119.
33. Donati, C.; Douglas, J.; Kob, W.; Plimpton, S.; Poole, P.; Glotzer, S. Stringlike Cooperative Motion in a Supercooled Liquid. *Phys. Rev. Lett.* **1998**, *80*, 2338–2341.
34. Zhang, H.; Kalvapalle, P.; Douglas, J. F. String-Like Collective Atomic Motion in the Interfacial Dynamics of Nanoparticles. *Soft Matter* **2010**, *6*, 5944–5955.
35. Zhang, H.; Srolovitz, D. J.; Douglas, J. F.; Warren, J. A. Grain Boundaries Exhibit the Dynamics of Glass-Forming Liquids. *Proc. Natl. Acad. Sci. U.S.A.* **2009**, *106*, 7735–7740.
36. Zhang, H.; Douglas, J. F. Glassy Interfacial Dynamics of Ni Nanoparticles: Part Ii Discrete Breathers as an Explanation of Two-Level Energy Fluctuations. *Soft Matter* **2013**, *9*, 1266–1280.
37. Zhang, H.; Douglas, J. F. Glassy Interfacial Dynamics of Ni Nanoparticles: Part I Colored Noise, Dynamic Heterogeneity and Collective Atomic Motion. *Soft Matter* **2013**, *9*, 1254–1265.
38. Starr, F. W.; Hartmann, B.; Douglas, J. F. Dynamical Clustering and a Mechanism for Raft-Like Structures in a Model Lipid Membrane. *Soft Matter* **2014**, *10*, 3036–3047.
39. Riggleman, R.; Yoshimoto, K.; Douglas, J.; de Pablo, J. Influence of Confinement on the Fragility of Antiplasticized and Pure Polymer Films. *Phys. Rev. Lett.* **2006**, *97*, 045502.
40. Wales, D. J.; Doye, J. P. K. Dynamics and Thermodynamics of Supercooled Liquids and Glasses from a Model Energy Landscape. *Phys. Rev. B* **2001**, *63*, 214204.
41. Keys, A. S.; Abate, A. R.; Glotzer, S. C.; Durian, D. J. Measurement of Growing Dynamical Length Scales and Prediction of the Jamming Transition in a Granular Material. *Nat. Phys.* **2007**, *3*, 260–264.
42. Dudowicz, J.; Freed, K. F.; Douglas, J. F. Fragility of Glass-Forming Polymer Liquids. *J. Phys. Chem. B* **2005**, *109*, 21350–21356.
43. Wales, D. J.; McKay, H.; Altschuler, E. L. Defect Motifs for Spherical Topologies. *Phys. Rev. B* **2009**, *79*, 224115.
44. Zhang, H.; Srolovitz, D. J.; Douglas, J. F.; Warren, J. A. Characterization of Atomic Motion Governing Grain Boundary Migration. *Phys. Rev. B* **2006**, *74*, 115404.
45. Mendelev, M. I.; Zhang, H.; Srolovitz, D. J. Grain Boundary Self-Diffusion in Ni: Effect of Boundary Inclination. *J. Mater. Res.* **2005**, *20*, 1146–1153.
46. Wales, D. J.; Berry, R. S. Coexistence in Finite Systems. *Phys. Rev. Lett.* **1994**, *73*, 2875–2878.
47. Wales, D. J.; Berry, R. S. Melting and Freezing of Small Argon Clusters. *J. Chem. Phys.* **1990**, *92*, 4283–4295.
48. Sun, D. Y.; Gong, X. G. Structural Properties and Glass Transition in Al-N Clusters. *Phys. Rev. B* **1998**, *57*, 4730–4735.
49. Wales, D. J. Instantaneous Normal Mode Analysis and Coexistence Phenomena in Small Clusters. *J. Chem. Soc. Faraday T.* **1991**, *87*, 2399–2405.
50. Kunz, R. E.; Berry, R. S. Coexistence of Multiple Phases in Finite Systems. *Phys. Rev. Lett.* **1993**, *71*, 3987–3990.
51. Berry, R. S. Melting and Freezing Phenomena. *Microscale Therm. Eng.* **1997**, *1*, 1–18.
52. Berry, R. S.; Smirnov, B. A. Observability of Coexisting Phases of Clusters. *Int. J. Mass Spectrom.* **2009**, *280*, 204–208.
53. Berry, R. S.; Smirnov, B. M. Bridging the Macro and Micro. *Chem. Phys. Lett.* **2013**, *573*, 1–4.
54. Wales, D. J.; Doye, J. P. K. Coexistence and Phase-Separation in Clusters - from the Small to the Not-So-Small Regime. *J. Chem. Phys.* **1995**, *103*, 3061–3070.
55. Zhang, H.; Kalvapalle, P.; Douglas, J. F. String-Like Collective Atomic Motion in the Melting and Freezing of Nanoparticles. *J. Phys. Chem. B* **2011**, *115*, 14068–14076.
56. Zhang, Z.; Li, J. C.; Jiang, Q. Modelling for Size-Dependent and Dimension-Dependent Melting of Nanocrystals. *J. Phys. D: Appl. Phys.* **2000**, *33*, 2653–2656.
57. Aguado, A.; Jarrold, M. F. Melting and Freezing of Metal Clusters. *Annu. Rev. Phys. Chem.* **2011**, *62*, 151–172.
58. Joshi, K.; Krishnamurty, S.; Kanhere, D. G. "Magic Melters" Have Geometrical Origin. *Phys. Rev. Lett.* **2006**, *96*, 135703.
59. Schmidt, M.; Kusche, R.; von Issendorff, B.; Haberland, H. Irregular Variations in the Melting Point of Size-Selected Atomic Clusters. *Nature* **1998**, *393*, 238–240.
60. Doye, J. P. K.; Wales, D. J. Global Minima for Transition Metal Clusters Described by Sutton-Chen Potentials. *New J. Chem.* **1998**, *22*, 733–744.
61. Noya, E. G.; Doye, J. P. K.; Wales, D. J.; Aguado, A. Geometric Magic Numbers of Sodium Clusters: Interpretation of the Melting Behaviour. *Eur. Phys. J. D* **2007**, *43*, 57–60.
62. Jellinek, J.; Beck, T. L.; Berry, R. S. Solid−Liquid Phase Changes in Simulated Isoenergetic Ar13. *J. Chem. Phys.* **1986**, *84*, 2783–2794.
63. Jellinek, J.; Goldberg, A. On the Temperature, Equipartition, Degrees of Freedom, and Finite Size Effects: Application to Aluminum Clusters. *J. Chem. Phys.* **2000**, *113*, 2570–2582.
64. Trygubenko, S. A.; Wales, D. J. Analysis of Cooperativity and Localization for Atomic Rearrangements. *J. Chem. Phys.* **2004**, *121*, 6689–6697.
65. Zhang, H.; Khalkhali, M.; Liu, Q. X.; Douglas, J. F. String-Like Cooperative Motion in Homogeneous Melting. *J. Chem. Phys.* **2013**, *138*, 12A538.
66. de Souza, V. K.; Wales, D. J. Energy Landscapes for Diffusion: Analysis of Cage-Breaking Processes. *J. Chem. Phys.* **2008**, *129*, 164507.
67. Wang, L.; Peng, C.; Wang, Y.; Zhang, Y. Relating Nucleation to Dynamical and Structural Heterogeneity in Supercooled Liquid Metal. *Phys. Lett. A* **2006**, *350*, 69–74.
68. Zhang, T. H.; Liu, X. Y. How Does a Transient Amorphous Precursor Template Crystallization. *J. Am. Chem. Soc.* **2007**, *129*, 13520–13526.
69. Posner, A. S.; Betts, F. Synthetic Amorphous Calcium Phosphate and Its Relation to Bone Mineral Structure. *Acc. Chem. Res.* **1975**, *8*, 273–281.
70. Deshpande, A. S.; Fang, P.-A.; Simmer, J. P.; Margolis, H. C.; Beniash, E. Amelogenin-Collagen Interactions Regulate Calcium Phosphate Mineralization *in Vitro*. *J. Biol. Chem.* **2010**, *285*, 19277–19287.
71. Dey, A.; Bomans, P. H.; Müller, F. A.; Will, J.; Frederik, P. M.; de With, G.; Sommerdijk, N. A. The Role of Prenucleation Clusters in Surface-Induced Calcium Phosphate Crystallization. *Nat. Mater.* **2010**, *9*, 1010–1014.
72. Fang, P.-A.; Conway, J. F.; Margolis, H. C.; Simmer, J. P.; Beniash, E. Hierarchical Self-Assembly of Amelogenin and the Regulation of Biomineralization at the Nanoscale. *Proc. Natl. Acad. Sci. U.S.A.* **2011**, *108*, 14097–14102.
73. Vidavsky, N.; Addadi, S.; Mahamid, J.; Shimoni, E.; Ben-Ezra, D.; Shpigel, M.; Weiner, S.; Addadi, L. Initial Stages of Calcium Uptake and Mineral Deposition in Sea Urchin Embryos. *Proc. Natl. Acad. Sci. U.S.A.* **2014**, *111*, 39–44.
74. Gower, L. B. Biomimetic Model Systems for Investigating the Amorphous Precursor Pathway and Its Role in Biomineralization. *Chem. Rev.* **2008**, *108*, 4551–4627.
75. Liu, Y.; Kim, Y. K.; Dai, L.; Li, N.; Khan, S. O.; Pashley, D. H.; Tay, F. R. Hierarchical and Non-Hierarchical Mineralisation of Collagen. *Biomaterials* **2011**, *32*, 1291–1300.
76. Jung, H. Y.; Chun, H.; Park, S.; Kang, S. H.; Ahn, C. W.; Kwon, Y. K.; Upmanyu, M.; Ajayan, P. M.; Jung, Y. J. Liquid Metal Nanodroplet Dynamics inside Nanocontainers. *Sci. Rep.* **2013**, *3*, 1–5.
77. Jose-Yacaman, M.; Gutierrez-Wing, C.; Miki, M.; Yang, D. Q.; Piyakis, K. N.; Sacher, E. Surface Diffusion and Coalescence of Mobile Metal Nanoparticles. *J. Phys. Chem. B* **2005**, *109*, 9703–9711.
78. Johnston, J. C.; Molinero, V. Crystallization, Melting, and Structure of Water Nanoparticles at Atmospherically Relevant Temperatures. *J. Am. Chem. Soc.* **2012**, *134*, 6650–6659.
79. Voter, A. F.; Chen, S. P. In *Accurate Interatomic Potentials for Ni, Al and Ni3al*; MRS Proceedings, Cambridge University Press: Cambridge, 1986.

80. Lee, S. G.; Chung, Y. C. Atomic-Level Investigation of Al and Ni Thin Film Growth on Ni(111) Surface: Molecular Dynamics Simulation. *Appl. Surf. Sci.* **2007**, *253*, 8896–8900.
81. Mishin, Y.; Farkas, D.; Mehl, M. J.; Papaconstantopoulos, D. A. Interatomic Potentials for Monoatomic Metals from Experimental Data and Ab Initio Calculations. *Phys. Rev. B* **1999**, *59*, 3393–3407.
82. Chen, S. P.; Voter, A. F.; Srolovitz, D. J. Oscillatory Surface Relaxations in Ni, Al, and Their Ordered Alloys. *Phys. Rev. Lett.* **1986**, *57*, 1308–1311.
83. Chamati, H.; Gaminchev, K. Crystallization of Nickel Nanoclusters by Molecular Dynamics. *J. Phys. Conf. Ser.* **2012**, 398.
84. Parks, E. K.; Zhu, L.; Ho, J.; Riley, S. J. The Structure of Small Nickel Clusters. Ii. Ni-16-Ni-28. *J. Chem. Phys.* **1995**, *102*, 7377–7389.
85. Parks, E. K.; Riley, S. J. Nickel Cluster Structure Determined from the Adsorption of Molecular Nitrogen - Ni-49-Ni-71. *Z. Phys. D Atom. Mol. Cl.* **1995**, *33*, 59–70.
86. Flory, P. *Principles of Polymer Chemistry*; Cornell University Press: Ithaca, 1953.
87. Simmons, D. S.; Cicerone, M. T.; Zhong, Q.; Tyagi, M.; Douglas, J. F. Generalized Localization Model of Relaxation in Glass-Forming Liquids. *Soft Matter* **2012**, *8*, 11455–11461.
88. Šolc, K. Shape of a Random Flight Chain. *J. Chem. Phys.* **1971**, *55*, 335–344.
89. Šolc, K.; Stockmayer, W. H. Shape of a Random-Flight Chain. *J. Chem. Phys.* **1971**, *54*, 2756–2757.
90. Šolc, K. Statistical Mechanics of Random-Flight Chains. Iv. Size and Shape Parameters of Cyclic, Star-Like, and Comb-Like Chains. *Macromolecules* **1973**, *6*, 378–385.
91. Mattice, W. L; Suter, U. W. *Conformational Theory of Large Molecules*; Wiley Interscience: New York, 1994.